Acta Materialia 266 (2024) 119687

Contents lists available at ScienceDirect

Acta Materialia

journal homepage: www.elsevier.com/locate/actamat

Full length article

Diffusion-controlled growth and microstructural evolution between Pt and Pd containing B2-NiAl bondcoats and Ni-based single crystal superalloy

Neelamegan Esakkiraja [a,b,*], Aditya Vishwakarma [c], Surendra K Makineni [a], Vikram Jayaram [a], Tilmann Hickel [c,d], Sergiy V. Divinski [b], Aloke Paul [a]

[a] Department of Materials Engineering, Indian Institute of Science, Bangalore 560012, India
[b] Institute of Materials Physics, University of Münster, Münster 48149, Germany
[c] Max–Planck-Institut für Eisenforschung GmbH, D-40237 Düsseldorf, Germany
[d] BAM Federal Institute for Materials Research and Testing, D-12489 Berlin, Germany

ARTICLE INFO

Keywords:
Interdiffusion
Bondcoat
TCP phase
TEM
APT

ABSTRACT

Pt-modified NiAl bond coats are used to extend the lifetime of blades in gas turbine engine applications. However, they suffer from the growth of deleterious precipitates within the interdiffusion zone. Partial substitution of Pt by Pd is advantageous in reducing the interdiffusion zone thickness between the bond coat and the superalloy, providing comparable oxidation properties, and critically reducing the propensity to form brittle $(Pt,Ni)Al_2$ precipitates. In this study, we utilize the pseudo-binary diffusion couple method to estimate the interdiffusion coefficients of Ni and Al in Pd, Pd-Pt and Pt-modified nickel aluminides. Additionally, the main and cross-interdiffusion coefficients are estimated in the ternary diffusion couples. The estimated diffusion coefficients in the β-NiAl phase reflect on the thickness of the β phase in the superalloy bond coat interdiffusion zone. Pd reduces the pseudo-binary interdiffusion coefficients of Ni–Al and also decreases the main and cross-ternary interdiffusion coefficients. This correlates with the reduction of the interdiffusion zone thickness by Pd. The diffusion process is strongly assisted by point defects in this phase. Ab initio-informed defect calculations are done to explain diffusion retardation in the presence of Pd (compared to Pt) with decreased defect concentrations. Furthermore, through in-depth microstructure characterization performed by electron probe micro analyser, transmission electron microscopy, and atom probe tomography, the presence of σ, R and μ phases as TCP precipitates in the interdiffusion zone are identified. The results give insights into the coatings' diffusional properties that influence the service life of the product.

1. Introduction

Platinized β-NiAl bond coats on Ni-based superalloys have been extensively used for decades. They act as Al-reservoir for the continuous growth of a protective α-Al_2O_3 layer, which reduces substantially the oxygen diffusion through the oxide layer [1]. Furthermore, the NiAl-based coating provides a bond with the yttria-stabilized zirconia topcoat for thermal protection in a harsh environment at operating temperatures. The addition of Pt improves the adherence of the oxide layer and thus increases the service life [2]. However, it brings a few unavoidable disadvantages. For example, a high volume fraction of the brittle $(Pt,Ni)Al_2$ intermetallic compound is formed near the initial surface, during the growth of the bond coat by a diffusion-controlled pack cementation process, which is deleterious for the structure [3]. The reason for the formation of this can be understood from the presence this $(Pt,Ni)Al_2$ phase in the Ni–Pt–Al phase diagram determined experimentally by Hayashi et al. [4] Moreover, Pt significantly enhances the diffusion rates of the elements between the superalloy and the bond coat. As a result, an enlarged interdiffusion zone (IDZ) also appears with a very high-volume fraction of brittle TCP (topologically closed packed) phases [5–8].

Continuous efforts for complete or partial replacement of Pt in the bond coat are being made in the research community. The addition of Pd brings certain benefits. For example, the Pd–Al system does not contain a phase equivalent to the $PtAl_2$ phase in the Pt–Al one, and the growth of such brittle precipitates can be avoided entirely [9–11]. Moreover, the growth of the interdiffusion zone also decreased dramatically [12]. Lamesle et al. [11] discussed the growth process of bond coat in the presence of Pd and PdNi precoating instead of Pt; however, without estimating the diffusion coefficients. Hayashi et al. [4] developed the Ni–Pt–Al phase diagram with the help of diffusion couples. However, they did not estimate the diffusion coefficients [4]. On the other hand, Adharapurapu et al. [13] studied the

* Corresponding author at: Institute of Materials Physics, University of Münster, Münster 48149, Germany.
E-mail address: eneelame@uni-muenster.de (N. Esakkiraja).

https://doi.org/10.1016/j.actamat.2024.119687
Received 24 August 2023; Received in revised form 12 January 2024; Accepted 14 January 2024
Available online 19 January 2024

effect of the addition of Pd+Hf and Pt+Hf to NiCrAl coating. This is another type of coating close to the NiCrAlY type in which the growth mechanism of the interdiffusion zone is different compared to the growth of the β-NiAl bond coat. Góral et al. [14] produced Pt–Pd–Hf–Zr containing coating to demonstrate only the methodology of producing such coating following a different method. Romanowska et al. [15] compared the performance between the Pd and Pd–Zr-doped coatings to find the beneficial role of the Zr doping. They did not compare the performance with the Pt-containing bond coats.

Despite the numerous available studies, a basic understanding of the physical phenomena responsible for the differences in the development of the interdiffusion zones in the presence of Pt or Pd, which accounts for the loss of Al from the bond coat is simply absent. An estimation of the diffusion coefficients in both the Ni–Pt–Al and Ni–Pd–Al diffusion couples is imperative to provide fundamental insights into the corresponding mechanisms.

An inferior cyclic oxidation resistance of the Pd-modified NiAl bond coat compared to the Pt-containing one has been reported recently [12]. Still, a partial replacement of Pt with Pd is proven beneficial without this obvious disadvantage. The cyclic oxidation resistance of the (Pt+Pd)-containing NiAl bond coat is comparable to the pure Pt-containing bond coat [12,16]. The deleterious $(Pt,Ni)Al_2$ precipitates did not grow in the pack cemented bond coat [16].

On the other hand, the effect of Pd on the growth of the interdiffusion zone between the superalloy and the bond coat is not studied in a correlation with the estimated diffusion coefficients, indicating the change in diffusion rates of elements because of complete or partial replacement of Pt with Pd. The growth of this interdiffusion zone containing different TCP (topologically close-packed) phases is unavoidable but undesirable, which leads to the unwanted loss of Al. In fact, the unwanted consumption of Al for the growth of the interdiffusion zone is far higher than the useful consumption of Al for the growth of the oxide layer [12] (see the Supplementary Material). This may affect the growth of the oxide layer after a long service life. Therefore, a comprehensive study on the growth of the interdiffusion zone is of utmost importance as it directly impacts the product's life. Moreover, the estimation of diffusion coefficients for a complete or partial replacement of Pt with Pd will be important for modelling the microstructure evolution in future. The experimental measurements must thus be combined with a detailed assessment of the impact of alloying elements on the defect concentrations, defect migration and alloy thermodynamics to provide an adequate understanding of the diffusion processes [7,17]. Such a correlation of diffusion and defect evolution is not yet established for the (Pt+Pd)-containing B2-NiAl bond coats in view of obvious computational complications for systems with more than three elements. Therefore, a state of the art ab-initio study is mandatory to accomplish these tasks, which has been missing until now.

A radiotracer method [18] in aluminides for estimating the diffusion coefficients of all the elements is challenging because of the very high costs of the only suitable ^{26}Al radioisotope with low specific activity. Moreover, suitable Pt and Pd radioisotopes with a reasonable half-life for the experiments are nowadays almost unavailable, again due to high costs. The availability of the required facilities is also very limited because of safety issues.

Alternatively, a diffusion couple method is widely practised for estimating diffusion coefficients in an inhomogeneous material system. However, until recently, no method was available for a systematic diffusion analysis to estimate the composition-dependent diffusion coefficients in a system with more than three elements. The recently proposed pseudo-binary diffusion couple method is the simplest but most useful diffusion analysis in a multi-component system [19,20]. In this study, we first estimate the diffusion coefficients following the pseudo-binary diffusion couple method, which indicates systematic changes in the concentration-dependent Ni–Al interdiffusion coefficients because of the addition of Pt, Pd or (Pt+Pd). The study is then extended, estimating the main and cross interdiffusion coefficients following the conventional ternary diffusion couple methods in the Ni–Pt–Al and Ni–Pd–Al ternary systems. The diffusion process in the β-NiAl phase is strongly influenced by the vacancy and anti-site defects on different sublattices [17]. Therefore, an ab-initio analysis is conducted to determine the changes in the defect concentrations on different sublattices in the presence of Pd instead of Pt. Finally, an in-depth analysis of the microstructure evolution in the interdiffusion zone is done by combining electron probe microanalyzer (EPMA), transmission electron microscopy (TEM) and atom probe tomography (APT) and correlating the results with the quantitative diffusion analysis.

Therefore, this study is focused on model pseudo-binary and ternary systems for estimation of the diffusion coefficients and correlation to the growth of the interdiffusion zone between the superalloy and the bond coat. This study is thus fundamental in nature, providing a comprehensive understanding of the underlying diffusion processes. A combined application of Pd and Pt is shown to bring significant benefits in reducing the unwanted loss of Al by reducing the growth of the interdiffusion zone. This indicates an overall benefit in support of previous findings of a very good spallation resistance of the thermally grown oxide layer [12,16] and avoiding the growth of unwanted brittle $(Pt,Ni)Al_2$ particles [16]. The change in concentration of point defects and migration energies calculated following the density functional theory explains the reason behind the decrease in the interdiffusion rate of Ni–Al to decrease the growth rate of the interdiffusion zone with a significant advantage of reducing the Al loss from the bond coat.

2. Methodology

2.1. Experimental procedure

The alloys were produced by arc melting under purified Ar atmosphere using pure elements of Ni (99.95 wt.%), Al (99.9 wt.%), Pd (99.95 wt.%) and Pt (99.99 wt.%) respectively. The melted alloy buttons were homogenized at 1473 K for 100 h in a tubular vacuum furnace at about $\approx 10^{-4}$ Pa pressure. Following, the compositions were measured at various points randomly selected by spot analysis in an EPMA. The compositions were determined to be within ± 0.1 at.% from the average compositions mentioned in Table 1.

Homogenized alloy buttons were sliced with desired dimensions ($5 \times 5 \times 1.5$ mm^3) by electro-discharge machining to produce the diffusion couple. The end-member alloys used for preparing different diffusion couples (DCs) are listed in Table 1. Diffusion couples' pairs are prepared using special fixtures made of high-temperature-resistant steel. The diffusion couples (DC-1 to DC-9) are mentioned in Table 1. The diffusion couples were annealed at 1373 K for 25 h in a vacuum furnace. After the annealing, the samples were allowed for air cooling instead of quenching to avoid damaging the diffusion couples in view of their extreme brittleness at the low temperatures. After removing the samples from the fixture, these were mounted in epoxy and cross-sectioned with a slow-speed cutting saw using the thin diamond blade (thickness of 0.25 mm). A standard metallographic procedure was then followed to prepare the samples for composition profile measurements in EPMA. All the measurements are done in JEOL JXA-8350F with a thermal field emission gun source using the acceleration voltage kept at 15 kV, and the probe current is maintained at 50 nA. Pure elements were used as the standards.

Following the diffusion couple method, a commercial CMSX-4 single crystal superalloy was used to grow the interdiffusion zone with Pd or Pt-containing bond coats. The average composition of the CMSX-4 superalloy is given in Table 2. After the diffusion annealing, the samples were cross-sectioned and prepared metallographically to examine the microstructure characteristics in scanning electron microscopy and EPMA. The precipitates were identified in 200 kV transmission electron microscopy (TEM) using FEI Tecnai T20-ST with LaB6 electron source. TEM Lamellae was prepared in the Focused Ion Beam (FIB)

Table 1
Desired compositions of the alloys and diffusion couple pairs. The diffusion couple pairs were annealed at 1373 K for 25 h.

Alloy designation	Composition (at.%)
EMPB-1	$Ni_{51.1}Pt_{9.5}Al_{39.4}$
EMPB-2	$Ni_{40.2}Pt_{9.3}Al_{50.5}$
EMPB-3	$Ni_{51.5}Pt_{9.1}Al_{39.4}$
EMPB-4	$Ni_{40.5}Pt_{9.1}Al_{50.4}$
EMPB-5	$Ni_{50.0}Pd_{10.1}Al_{39.9}$
EMPB-6	$Ni_{40.4}Pd_{10.1}Al_{49.5}$
EMPB-7	$Ni_{50.4}Pd_{15.1}Al_{34.5}$
EMPB-8	$Ni_{35.8}Pd_{15.1}Al_{49.1}$
EMPB-9	$Ni_{50.2}Pd_{5.0}Pt_{4.9}Al_{39.9}$
EMPB-10	$Ni_{40.7}Pd_{5.1}Pt_{4.9}Al_{49.3}$
EMT-1	$Ni_{51.6}Pt_{10.1}Al_{38.4}$
EMT-2	$Ni_{44.9}Pt_{5.8}Al_{49.3}$
EMT-3	$Ni_{54.5}Pt_{5.7}Al_{39.8}$
EMT-4	$Ni_{40.8}Pt_{10.3}Al_{48.9}$
EMT-5	$Ni_{50.3}Pd_{10.3}Al_{39.4}$
EMT-6	$Ni_{45.2}Pd_{5.2}Al_{49.6}$
EMT-7	$Ni_{54.6}Pd_{5.1}Al_{40.3}$
EMT-8	$Ni_{39.4}Pd_{10.0}Al_{50.6}$
Diffusion couple designation	**Alloy combination**
DC-1	EMPB-1/EMPB-2
DC-2	EMPB-3/EMPB-4
DC-3	EMPB-5/EMPB-6
DC-4	EMPB-7/EMPB-8
DC-5	EMPB-9/EMPB-10
DC-6	EMT-1/EMT-2
DC-7	EMT-3/EMT-4
DC-8	EMT-5/EMT-6
DC-9	EMT-7/EMT-8
DC-10	EMPB-4/CMSX-4
DC-11	EMPB-8/CMSX-4
DC-12	EMPB-10/CMSX-4
DC-13	EMPB-6/CMSX-4

Table 2
Composition of the superalloy (CMSX-4). The concentrations of other elements, such as Y, Zr, Hf, S, C, O and P, are at the ppm levels.

Elements (at.%)	Co	Cr	Al	Ti	Ta	Mo	W	Re	Ni
CMSX-4	8.7	7.1	11.8	1.2	2	0.3	1.8	1	66

Helios G4-UX DualBeam equipped with a field emission electron gun source for imaging and a Ga Ion beam source for the milling procedure. The standard in-situ lift-out procedure is used for welding the lamellae in TEM-FIB grid, here the gas injection system (GIS) attached to the FIB equipment was used for deposition and welding purposes in FIB. CAMECA LEAP 5000XR Atom Probe Tomography (APT) was used to identify the chemical composition of the matrix in the precipitate containing interdiffusion zone.

2.2. Computational procedure

The point defect energies are calculated using a similar density functional theory (DFT) scheme as proposed previously [7]. The projector augmented wave (PAW) method as implemented in the Vienna Ab initio Simulation Package (VASP) [21,22] was utilized and the calculations were performed spin-polarized. The electronic exchange and correlation effects were considered within the generalized gradient approximation (GGA) using the Perdew, Burke and Ernzerhof (PBE) parameterization scheme [23]. The integration over the Brillouin zone was performed using the Monkhorst–Pack scheme [24] with a $4 \times 4 \times 4$ reciprocal-space k-mesh (for a $4 \times 4 \times 4$ repetitions (128 atoms) of the bcc conventional unit cell) centred around the Γ point and utilizing the Methfessel–Paxton scheme [25] with a thermal smearing width of 0.15 eV to account for the smoothening of partial occupancies of electronic states. The plane-wave energy cutoff was set to 400 eV. An energy of 10^{-7} eV was used as a convergence criterion for the self-consistent electronic loop [7].

3. Results and discussion

3.1. Microstructural analysis

As shown in Fig. 1, the interdiffusion zone growth between Pt, Pd and (Pt+Pd) containing β-NiAl bond coat and CMSX-4 superalloy is studied following the diffusion couple method that mimics the growth of IDZ in the actual structure during the service. IDZ has two parts, precipitate-containing and precipitate-free, which are demarcated by the dashed line in Fig. 1. The precipitate-containing IDZ is visible in the BSE image. The extent of precipitate-free IDZ can be realized from the elements' diffusion (composition) profiles. The unaffected bond coat end-member alloys in all the diffusion couples are further away from the right-hand side of the image, as indicated by arrows. The total thickness of IDZ is significantly smaller in the presence of Pd (Fig. 1a) instead of Pt (Fig. 1d) in the β-NiAl bond coat. In the presence of both Pt and Pd with equal concentrations (Fig. 1c), the IDZ thickness is higher than the IDZ for the purely Pd-containing bond coat but lower than the Pt-containing bond coat. As already mentioned, in the presence of Pd instead of Pt, deleterious $(Pt,Ni)Al_2$ phase does not grow during the pack cementation process [16] of bond coat growth. However, it deteriorates the oxide spallation resistance [26]. On the other hand, in the presence of both Pt and Pd in equal concentration, the spallation resistance of the oxide is good [12] without growing the $(Pt,Ni)Al_2$ phase [16]. Therefore, the addition of both Pt and Pd is preferable. This imparts the benefit of thickness reduction of the deleterious precipitate-containing IDZ as well.

In all the diffusion couples, the thickness of the precipitate-containing IDZ is much lower than that of the precipitate-free IDZ. The change in thickness with the change in alloying elements (Pd and Pt) is more prominent in the precipitate-free IDZ. The dotted line in Fig. 1 indicates the position of the Kirkendall marker plane, which can be understood from the microstructure evolution on either side of the Kirkendall plane and by the presence of a line of pores along it. Both methods, i.e. by locating the plane corresponding to specific microstructure differences or by direct observation of a line of pores, are known to provide reliable detection of the position of the Kirkendall marker plane [27,28]. Thus, the position of the Kirkendall plane indicates that the precipitate-containing IDZ grows from the superalloys, and the precipitate-free IDZ grows from the bond coat end-member.

Fig. 2 shows the enlarged BSE images of the precipitate-containing IDZ grown between the CMSX-4 superalloy and EMPB-4 ($NiPt_{10}Al_{50}$) diffusion couple annealed at 1373 K for 25 h. Note that the volume fraction of γ' is much higher than that of γ in the superalloy. The γ-phase is relatively brighter than the γ'-phase in the BSE image since the refractory alloying elements with higher atomic numbers preferentially partition towards the γ-phase. Ni, Co, Cr diffuse out from the superalloy, which is relatively rich in these phases compared to the bond coat. Similarly, the bond coat loses Al and Pt by diffusion in the opposite direction. With the loss of Ni, Co, Cr etc. or gain of Al, the superalloy with a phase mixture of γ-(Ni,Al,X) solid solution and γ'-$(Ni,X)_3(Al,Y)$ (where X and Y are the alloying elements, i.e. Cr, Co, Ta, Re, W etc.) first converts to a γ'-$(Ni,X)_3(Al,Y)$ and β-(Ni,X)(Al,Y) phase mixture and then with a further loss it converts to the β-(Ni,X)(Al,Y)-phase. The thickness of the γ'- and β- phase mixture region is much smaller than the β-(Ni,X)(Al,Y)-phase region. The solubility range of certain high-temperature refractory elements, such as Re, W, Ta etc. is lower in the β-phase than the γ and γ'-phases. This is evident from the growth of precipitates in the β-phase with a relatively high concentration of these elements, as it follows from the measured composition of the β-phase,

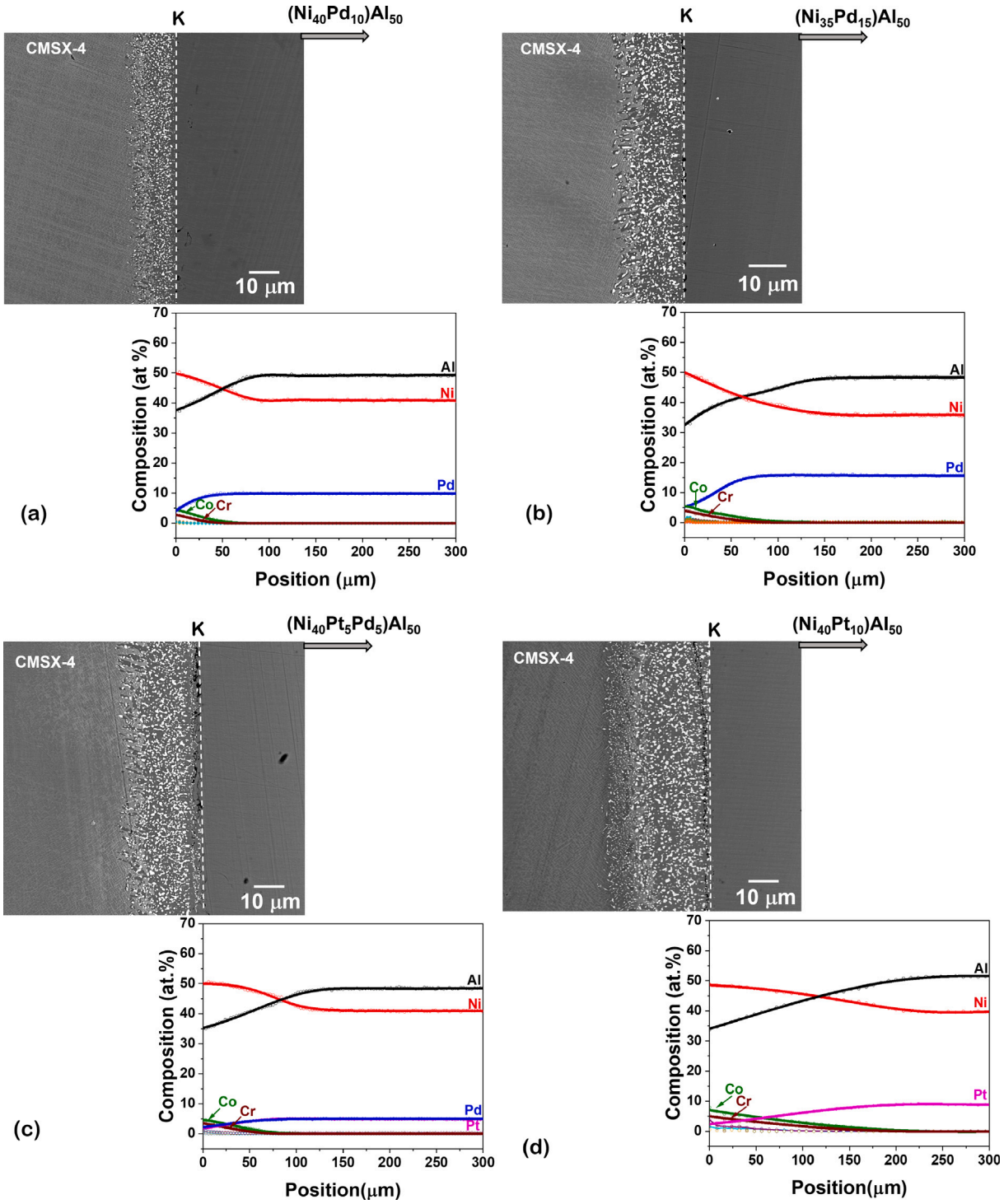

Fig. 1. Interdiffusion zone developed between CMSX-4 Superalloy and bond coat alloys (a) DC-13 (b) DC-11 (c) DC-12 (d) DC-10 and corresponding composition profiles at 1373 K for 25 h, dotted line demarcate the interdiffusion zone developed from superalloy and bond coat. The Kirkendall plane, "K", is indicated by dotted lines.

see below. In the $\gamma'+\beta$ phase mixture region, the precipitates are located at the β/γ' interfaces and grow inside the matrix.

The composition profile measured on another side of the Kirkendall marker plane indicates that Co and Cr diffuse towards the precipitate-free IDZ. The diffusion of other high-melting point refractory elements, such as Re, W, Ta etc., is found to be negligible. Pd/Pt and Al diffuse out from the bond coat end-member. Moreover, the diffusion length of Al in this part is found to be slightly higher than Ni and Pt but much higher than Pd.

The composition distribution is mapped in the precipitate-containing IDZ using EPMA, since the elemental distribution cannot be understood from line profiles in this zone. A very similar elemental distribution is found in the presence of Pt, Pd or (Pt+Pd), and one such example of the Pt-containing bond coat is shown in Fig. 3. The precipitates are lean in Ni and Al compared to the β-phase matrix and relatively rich in Co, Cr, W, Re etc. However, because of the final probe size and a high interaction volume (about cubic micrometre), the EPMA analysis does not provide an exact composition distribution of the matrix or precipitates.

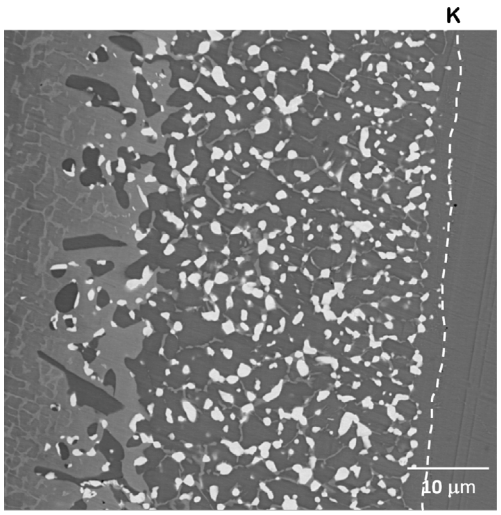

Fig. 2. BSE image showing the Kirkendall plane and the TCP precipitates grown in the interface between superalloy and EMPB-4 ($NiPt_{10}Al_{50}$) diffusion couple annealed at 1373 K for 25 h. The Kirkendall plane, "K", is indicated by dotted line.

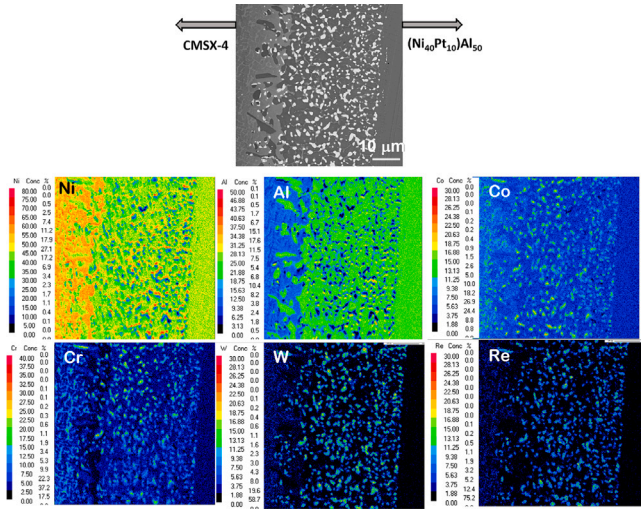

Fig. 3. The WDS elemental mapping indicates that the precipitates formed at the interface between CMSX-4 and EMPB-4 ($NiPt_{10}Al_{50}$) consist of a high concentration of refractory elements.

An atom probe tomography analysis is performed to determine the compositions of the γ'- and β-phases in the precipitate-containing IDZ, shown in Fig. 4. Re is found at the impurity level, whereas W and Ta in the grey γ'-phase is present with relatively higher amounts. However, the concentrations of these elements are found to be even lower in the dark β-phase. On the other hand, the bright TCP precipitates are very rich in these refractory elements.

The averaged (overall) distribution of the alloying elements, including that for Al, are represented by the diffusion profiles given for the precipitate-free interdiffusion zone in Fig. 1 and by the EPMA composition maps for the precipitate-containing interdiffusion zone including the superalloy adjacent to it in Fig. 3 (the distributions of all elements are shown in more details in the Supplementary Material, Fig. S3.

The APT analysis also indicates that Pt and Pd diffuse to the precipitate-containing interdiffusion zone with a much smaller concentration (within 2–3 at.%). The EPMA composition map, as shown in Fig. 5 verifies that the presence of these elements in the superalloy adjacent to the interdiffusion zone is negligible.

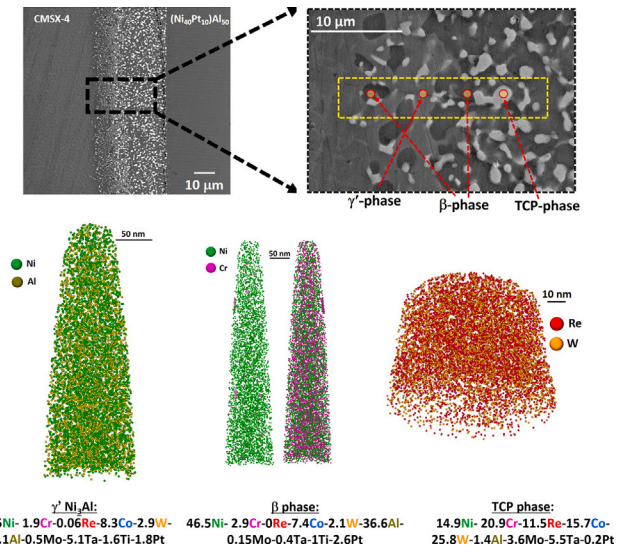

Fig. 4. APT reconstruction showing the composition distributions of the γ', β and TCP phases. The phase compositions are specified in at.%.

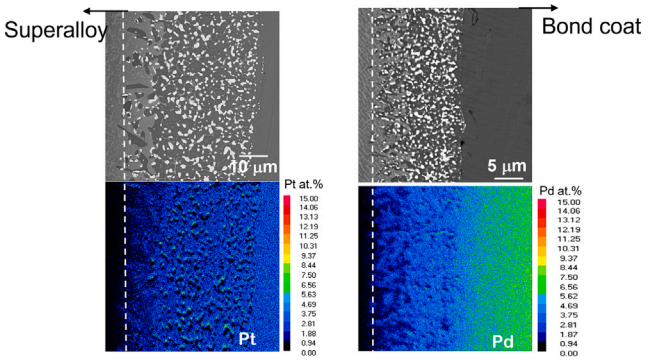

Fig. 5. The WDS elemental map of Pt and Pd indicating that the presence of these elements inside the CMSX-4 superalloy is negligible.

A TEM analysis examines the types of TCP phases present, as shown in Fig. 6. We found that the presence of Pt or Pd does not influence the types of precipitates grown in the IDZ. Three types of precipitates, σ, μ and R are found, and the details related to the crystal structure of these precipitates are listed in Table 3.

Following, a quantitative diffusion analysis is performed to understand the differences in the growth kinetics of the IDZ in the presence of Pd or Pt.

3.2. Quantitative diffusion analysis

3.2.1. Pseudo-binary diffusion couples

An accurate quantitative diffusion analysis is challenging or, rather, impossible in the IDZ that is grown between the superalloy and the bond coat because of a very complex compositional distribution in different phases. Estimating the diffusion coefficient in a phase mixture has no sense since the diffusion coefficients are specific for particular phases and compositions. The diffusion coefficient estimation in the precipitate-free IDZ is also difficult since an accurate average concentration profile in the interdiffusion zone (especially in the precipitate-containing zone) cannot be determined correctly. Even intersecting ($n-1$) diffusion paths by producing the diffusion profiles of all the elements in n component system (depending on the number of elements present in the superalloy and bond coat) is impossible since n is significantly larger than three [27,30].

Table 3
Crystallography details of the TCP precipitates identified in IDZ between superalloy and bondcoat [29].

TCP phase	Crystal system	Space group	Space group no	Atoms per unit cell	Lattice parameter	α(°)
σ	Tetragonal	P4/mnm	136	30	$a = 0.912,\ c = 0.472$	90
μ	Rhombohedral	R-3 m	166	13	$a = 0.473, c = 2.554$	120
R	Rhombohedral	R-3	148	53 (hex. 159)	$a = 1.093, c = 1.934$	120

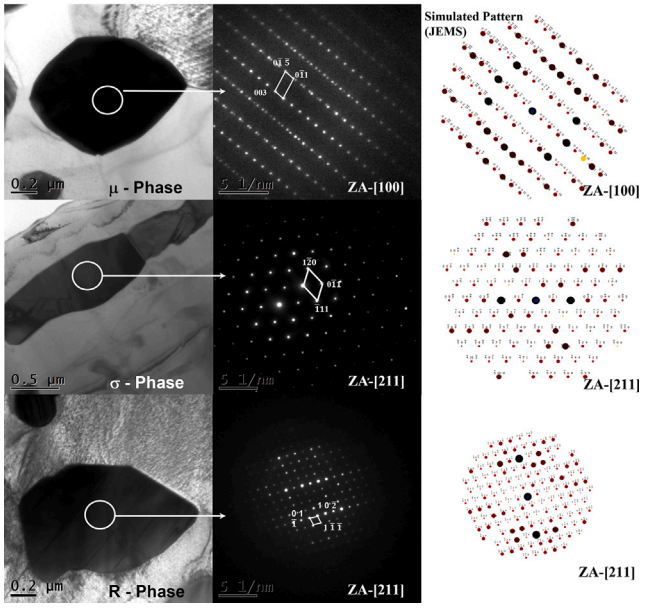

Fig. 6. Bright field image and selected area electron diffraction (SAED) patterns of the TCP phases found in the interdiffusion zone between the bond coat and CMSX-4 superalloy.

However, a quantitative diffusion analysis examining the change in the interdiffusion rates of mainly Ni and Al in the presence of Pt or Pd or both (Pt+Pd) in the β-NiAl can explain the growth characteristics of the β-phase in the superalloy/bond coat diffusion couple, too. The higher the diffusion rates of elements through this phase is, the higher is the growth rate of this phase by consuming the neighbouring phases (if the process is thermodynamically promoted). This argumentation becomes clearer if one follows the physico-chemical approach established by one of co-authors [27,28], explaining the growth of a phase by consuming the neighbouring phases in dependence on the diffusion rates in the product phase of interest and the thermodynamic equilibrium.

Note that a specific crystal orientation relationships between an fcc substrate and a bcc coating may affect the diffusion phenomena. Both experimentally [31] and theoretically [32,33] it was shown that diffusion-induced stresses might influence the intermixing rates, preserving the parabolic growth rate. The hydrostatic component of the stress tensor was considered in those analyses [32,33]. Due to a crystallographic anisotropy of the lattices, a minor impact of the crystal orientation on the interdiffusion rate might be expected as a third-order (probably not measurable) effect. However, this most likely will not affect the *relative* impacts of Pt or Pd alloying on the diffusion behaviour in a measurable way because of the similarity of the electronic configurations and the atomic radii.

With this aim, the recently established pseudo-binary (PB) diffusion couple method for ternary and multi-component systems is a suitable approach to practice in which the change of Ni–Al interdiffusion coefficients can be systematically estimated in the presence of Pt, Pd or (Pt+Pd). First, to produce a Pt-constant PB diffusion couple, two end-member alloys are intended to prepare with the same composition of Pt. However, when the diffusion couple was produced with these alloys as a first trial, as shown in Fig. 7a, one minor kink was found in the Pt composition profile instead of remaining constant (as circled with a dashed line). A close look at the two ends of the diffusion couple DC 1 produced by alloys EMPB-1 and EMPB-2 (see Table 1) indicated a small difference of 0.2 at.% of Pt at two end member alloys. This is one of the issues which may be faced during the PB diffusion couple experiments, which can be solved by correcting the end-member alloy(s). Therefore, another diffusion couple was prepared to match the Pt content in the end-member alloys, i.e. by coupling EMPB-3 and EMPB-4 alloys to produce a constant composition of Pt in the interdiffusion zone, as shown in Fig. 7b.

The PB interdiffusion coefficient, $\tilde{D}_{\mathrm{PB}}$, can be estimated using relations [7,19,20]

$$V_m \tilde{J}_{i,\mathrm{PB}} = -\tilde{D}_{\mathrm{PB}} \frac{dM_i}{dx} \tag{1}$$

and

$$V_m \tilde{J}_{i,\mathrm{PB}} = -\frac{(M_i^+ - M_i^-)}{2t} \left[\left(1 - Y^*_{i,\mathrm{PB}}\right) \int_{x^{-\infty}}^{x^*} Y_{i,\mathrm{PB}}\, dx + Y^*_{i,\mathrm{PB}} \int_{x^*}^{x^{+\infty}} \left(1 - Y_{i,\mathrm{PB}}\right) dx \right] \tag{2}$$

where $\tilde{J}_{i,\mathrm{PB}}$ is the PB interdiffusion flux of element i (= Ni or Al) calculated from modified composition (M_{Ni}) of elements related to the composition (N_i) of elements in mole or atomic fraction by i.e. $M_{\mathrm{Ni}} = N_{\mathrm{Ni}} + N_{\mathrm{Pt}}$ and $M_{Al} = N_{Al}$ since Pt occupies the Ni-sublattice, as explained in the ab-intio study described in the next section. $Y_{i,\mathrm{PB}} = (M_i - M_i^-)/(M_i^+ - M_i^-)$ is the modified composition normalized variable, $M_i^+ and M_i^-$ are the modified compositions at unaffected part of right- and left-hand side of the diffusion couple, V_m is the (constant) molar volume, which does not have to be calculated, x is the position parameter, t is the annealing time of the diffusion couple. It should be noted here that the PB interdiffusion coefficients estimated from the composition profile of Al or Ni or (Ni+Pt) give the same value (as in conventional binary case [27]). The PB interdiffusion coefficient of Ni and Al in the presence Pt is shown in Fig. 8. It should be noted here that since we have $M_{\mathrm{Ni}} + M_{\mathrm{Al}} = 1$ and $\tilde{J}_{i,\mathrm{PB}}$ estimated from modified composition profile of Ni and Al are related by $\tilde{J}_{\mathrm{Ni,PB}} + \tilde{J}_{\mathrm{Al,PB}} = 0$.

Next, a similar experiment is conducted in the Ni–Pd–Al system. As shown in Fig. 9(a), a diffusion couple is produced by coupling alloys EMPB-5 and EMPB-6. Although the composition of Pd in both the end member alloys is kept the same, a minor uphill diffusion profile of Pd is produced, Fig. 9(b).

This is another type of problem with PB diffusion couple which can be witnessed in certain systems. A diffusion profile of an element may or may not remain constant even when the end member alloys are produced with the same composition at two ends (with the accuracy of, let us say, ±0.1 at.%, which EPMA can detect). This behaviour cannot be considered a perfect or an ideal PB diffusion couple. If the non-ideality, i.e. the extent of uphill diffusion is small (like in this case), one may still calculate the PB interdiffusion coefficients by readjusting the composition profiles for utilization of the equation scheme valid for the PB diffusion couple, in fact by *forcing* the PB conditions. We first need to consider a constant value of Pd composition in the interdiffusion zone and then readjust the Ni and Al composition profiles such that we have $N_{\mathrm{Ni}} + N_{\mathrm{Al}} + N_{\mathrm{Pd}(const)} = 1$. Then only, we can estimate the composition-dependent PB interdiffusion coefficients from a PB diffusion couple [35,36].

However, the proposed readjusting of the diffusion profiles introduces an error in the calculations. This error can be significant only when the extent of the uphill diffusion profile of the element is high

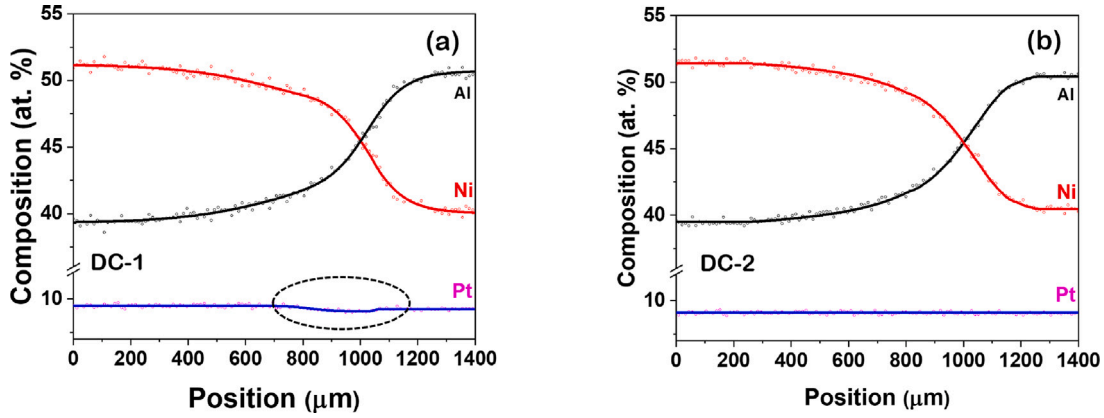

Fig. 7. Composition profiles developed for the PB couple with Pt remain as constant at 1373 K for 25 h of diffusion annealing: (a) DC-1 and (b) DC-2.

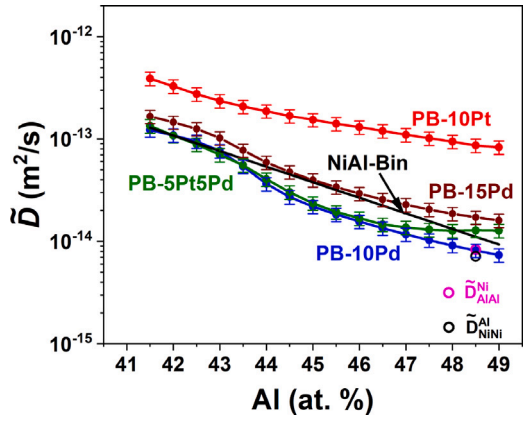

Fig. 8. PB interdiffusion coefficients of Ni and Al estimated at 1373 K with 10Pd (blue), 10Pt (red) or 5Pt+5Pd (green) additions (filled symbols). The $\tilde{D}^{Ni}_{AlAl}$ (magenta) $\tilde{D}^{Al}_{NiNi}$ (black) main interdiffusion coefficients measured using conventional Matano-Kirkaldy method [34] at one composition (open symbols). Pd and/or Pt free NiAl binary (Black line) [6,7]. (For interpretation of the references to colour in this figure legend, the reader is referred to the web version of this article.)

instead of remaining constant. In this example, as it can be seen in Fig. 9(c), the differences between the actual and readjusted (forced) diffusion profiles of Ni and Al are negligible. Therefore, the PB interdiffusion coefficient can be estimated without introducing any significant error. An exact analysis of the introduced errors and the deviations that may be considered acceptable is the subject of a separate (numerical) study, which is still in progress. However, this can also be cross-checked by comparing the PB interdiffusion coefficient and the interdiffusion coefficient estimated at the composition of the peak (zero gradient point) of the Pd uphill diffusion profile by considering it as a ternary diffusion couple.

Using a standard analysis for any ternary diffusion couple [27], one can determine the interdiffusion fluxes of the elements using the measured composition profiles. For a reference, the corresponding equations are given in the Supplementary Material, Eqs. (S1)–(S4).

Then, considering Al as the dependent variable, we can express the interdiffusion flux of Ni as a product of the corresponding interdiffusion matrix and the vector of composition gradients,

$$V_m \tilde{J}_{Ni} = -\tilde{D}^{Al}_{NiNi} \frac{dN_{Ni}}{dx} - \tilde{D}^{Al}_{NiPd} \frac{dN_{Pd}}{dx}. \quad (3)$$

Similarly, considering Ni as the dependent variable, the interdiffusion flux of Al can be expressed as

$$V_m \tilde{J}_{Al} = -\tilde{D}^{Ni}_{AlAl} \frac{dN_{Al}}{dx} - \tilde{D}^{Ni}_{AlPd} \frac{dN_{Pd}}{dx}. \quad (4)$$

At any extreme of the non-monotonous (uphill-affected) Pd composition profile, we have $dN_{Pd}/dx = 0$. Therefore, we can estimate the $\tilde{D}^{Al}_{NiNi}$ or $\tilde{D}^{Ni}_{AlAl}$ from the calculated interdiffusion flux at this composition. On the other hand, when we consider a constant diffusion profile of Pd instead of considering the actual diffusion profile with an uphill diffusion, the difference in $\tilde{D}_{PB}$ and $\tilde{D}^{Al}_{NiNi}$ or $\tilde{D}^{Ni}_{AlAl}$ estimated at the peak composition indicates obviously the error in the calculation of the PB interdiffusion coefficient. These values are compared in Fig. 8. This difference is found to be within typical experimental uncertainties and, therefore, the non-ideality of the PB diffusion couple in this system can be considered insignificant. A similar PB diffusion couple was prepared with 15 at.% Pd in both the end members. The PB interdiffusion coefficients are found to increase with Pd content from 10 to 15 at.%, as shown in Fig. 8.

Next, a PB diffusion couple was prepared with almost equal amounts of Pd and Pt in both the end members, i.e., by coupling the alloys EMPB-9 and EMPB-10. Previous experiments revealed that solely added Pt and Pd show different behaviours. In fact, Pt – *const* results in an ideal PB profile, while Pd–*const* produces a minor uphill feature, as shown in Figs. 7 and 9. However, as shown in Fig. 10, with the addition of both Pt and Pd simultaneously, a minor uphill effect is present. Since the extent of the uphill diffusion features is minor for both the elements, we can calculate the PB diffusion coefficients of Ni and Al by considering a constant diffusion profile and readjusting the Ni and Al diffusion profile accordingly so that we have $N_{Ni} + N_{Al} + N_{Pt(const.)} + N_{Pd(const.)} = 1$. This brings a minor but negligible difference in the Ni and Al diffusion profiles, considering which the PB interdiffusion coefficients are estimated. The determined variation of PB interdiffusion coefficients with the composition is plotted in Fig. 8. It is clear that the PB interdiffusion coefficients decrease when we replace Pt with Pd partially or completely.

The present analysis does not explicitly include the stresses. Thus, a full stress relaxation via plastic events in both fcc and bcc matrices is assumed [27]. We have verified the diffusion-controlled regime of the IDZ growth in the present case, see Fig. S5 in the Supplementary Material, and we conclude that the specific crystallographic orientation relations between the parent and product phases do not affect the growth process in view of the diffusion isotropy in the cubic phases. Note that similar results were observed, e.g., by Seyring and Rettenmayr for growth of the product Ni_3Al phase in the Ni/NiAl diffusion couple [37]. Definitely, precipitation of the TCP phases might depend on the particular orientation relationships, see the results of an EBSD analysis of the interdiffusion zone shown in Fig. S6 in the Supplementary Material, but a detailed analysis is out of the scope of the present analysis.

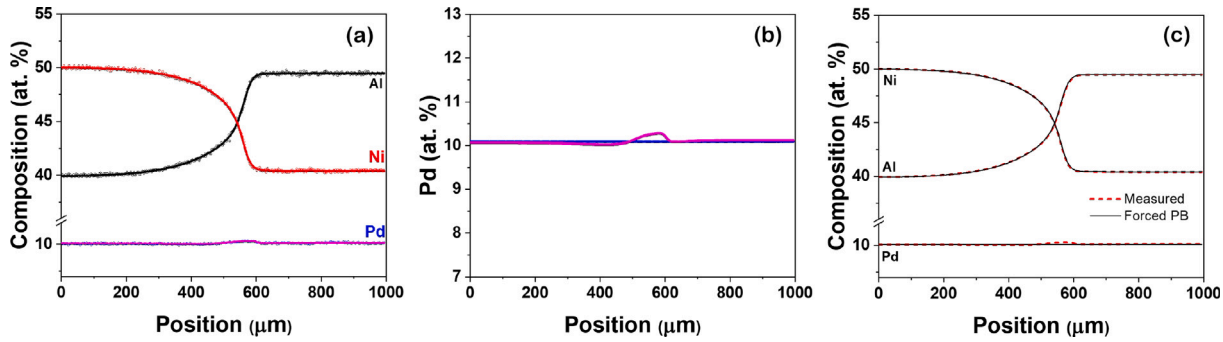

Fig. 9. (a) Composition profiles developed for the PB couple with Pd remain constant at 1373 K for 25 h; (b) enlarged Pd profile; (c) modifications of the concentration profiles by forcing the PB conditions.

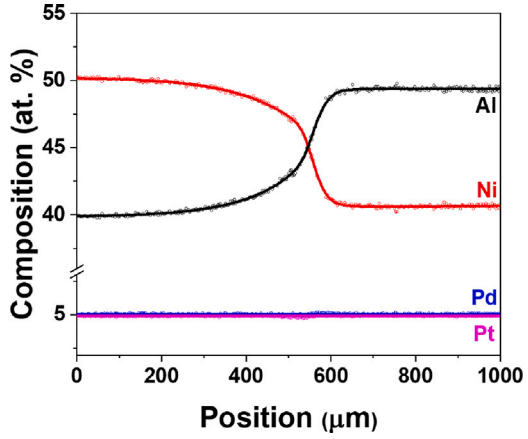

Fig. 10. Composition profiles developed for DC-5 at 1373 K for 25 h.

3.2.2. *Ternary diffusion couples*

An analysis of the determined PB interdiffusion coefficients indicates systematic changes in the interdiffusion coefficients of Ni and Al in the presence of Pt, Pd or (Pt+Pd) over the whole composition range of the diffusion couple. However, such a diffusion analysis does not provide a quantitative assessment of the diffusional interactions between Ni (and/or Al) and Pt (or Pd). Therefore, a further analysis was performed by applying the Ni–Pt–Al and Ni–Pd–Al ternary systems by producing ternary diffusion couples.

Fig. 11(a,b) shows the concentration profiles developed in the two diffusion couples, DC-6 and DC-7, produced by coupling the EMT-1/EMT-2 and EMT-3/EMT-4 alloys (see Table 1), respectively. The composition of the intersection can be found by plotting the diffusion paths on the Gibbs triangle, Fig. 11(c). The equation scheme used to determine the ternary main and cross interdiffusion coefficients is given in the Supplementary Material, Eqs. (S1)–(S4). We can write two independent equations correlating the interdiffusion fluxes and the composition gradients, which are related to four unknown interdiffusion coefficients. Therefore, we can estimate these interdiffusion coefficients at the composition of the intersection from two diffusion couples. Since Ni and Pt occupy the same sublattice, we have estimated the interdiffusion coefficients considering Al as the dependent variable such that we can compare the effect of Pt (or Pd) addition on the main and cross interdiffusion coefficients of Ni.

A note is due here. One can also estimate the interdiffusion coefficients considering Pt (Pd) or Ni as the dependent variables. The interdiffusion coefficients estimated considering different elements as the dependent variables are related [27,38]. The estimated interdiffusion coefficients in the Ni–Pt–Al system are listed in Table 4.

Table 4
The main and cross interdiffusion coefficients (in 10^{-15} m^2/s) estimated at the intersection of two independent diffusion paths, see the Gibbs triangle in Fig. 11(c) and Figs. 12(c).

Ni–Pt–Al	$\tilde{D}^{Al}_{NiNi}$	$\tilde{D}^{Al}_{NiPt}$	$\tilde{D}^{Al}_{PtPt}$	$\tilde{D}^{Al}_{PtNi}$
	50.5	32.1	4.95	0.065
Ni–Pd–Al	$\tilde{D}^{Al}_{NiNi}$	$\tilde{D}^{Al}_{NiPd}$	$\tilde{D}^{Al}_{PdPd}$	$\tilde{D}^{Al}_{PdNi}$
	38.5	30.3	4.17	1.72

An equivalent set of diffusion couples, i.e., DC-8 and DC-9, were produced in the Ni–Pd–Al system by coupling the EMT-5/EMT-6 and EMT-7/EMT-8 alloys (see Table 1). The results are presented in Fig. 12.

A direct comparison of the diffusion profiles in the Ni–Pt–Al and Ni–Pd–Al systems provides further insights into interdiffusion kinetics. One may note almost similar characteristics of the diffusion profiles although with different interdiffusion zone thicknesses and certain other differences in Pd- or Pt-bearing alloys when alloys with similar compositions are coupled, of DC-6 and DC-8 or DC-7 or DC-9 in Figs. 11 and 12, respectively.

The estimated interdiffusion coefficients are listed in Table 4. The main interdiffusion coefficient of Ni, $\tilde{D}^{Al}_{NiNi}$, is much higher than the main interdiffusion coefficient of Pt, $\tilde{D}^{Al}_{PtPt}$ (or Pd, $\tilde{D}^{Al}_{PdPd}$). Moreover, the main interdiffusion coefficient of Ni in the Ni–Pt–Al system is higher than the main interdiffusion coefficient of Ni in the Ni–Pd–Al system. This is the reason for a lower IDZ thickness in the presence of Pd compared to the presence of Pt (see Fig. 1). As already discussed, the thickness of the precipitate-free IDZ is much larger than the precipitate-containing IDZ in all the diffusion couples, which was also a common observation in other superalloy bond coat couples [6,7,39]. This can be because of the high volume fraction of precipitates in the precipitate containing IDZ, which are rich in high-melting point refractory elements such as Re, W, Mo, Ta, etc. Therefore, the effective area for interdiffusion of Ni and Al through the B2-NiAl is less than the precipitate-free IDZ, and the diffusion rate of the elements through the precipitates is very low. Moreover, these elements are also present in the precipitate-containing B2-NiAl matrix to reduce the interdiffusion rates. As already shown in Fig. 8, we noticed that the PB interdiffusion coefficient increases with the increase in Pd content from 10 at.% Pd to 15 at.% Pd. To check if we have a similar effect on the growth of IDZ between the bond coat and the superalloy, bond coats with 10 at.% Pd and 15 at.% Pd were coupled with CMSX-4. As can be seen in Fig. 1(a) and (b), the IDZ thickness with a bond coat of 15 at.% Pd is found to be higher than the thickness with a bond coat of 10 at.% Pd.

One may note that grains are generally very large in the precipitate-free interdiffusion zone that is grown from the bond coat alloy. Smaller grains can grow in the interdiffusion zone part that is grown from the superalloy, especially during the initial stages of the interdiffusion process, but the presence of TCP-precipitates blocks likely a potential contribution of the grain boundaries to the total diffusion transport. Accounting for the measured grain size and the relatively high diffusion

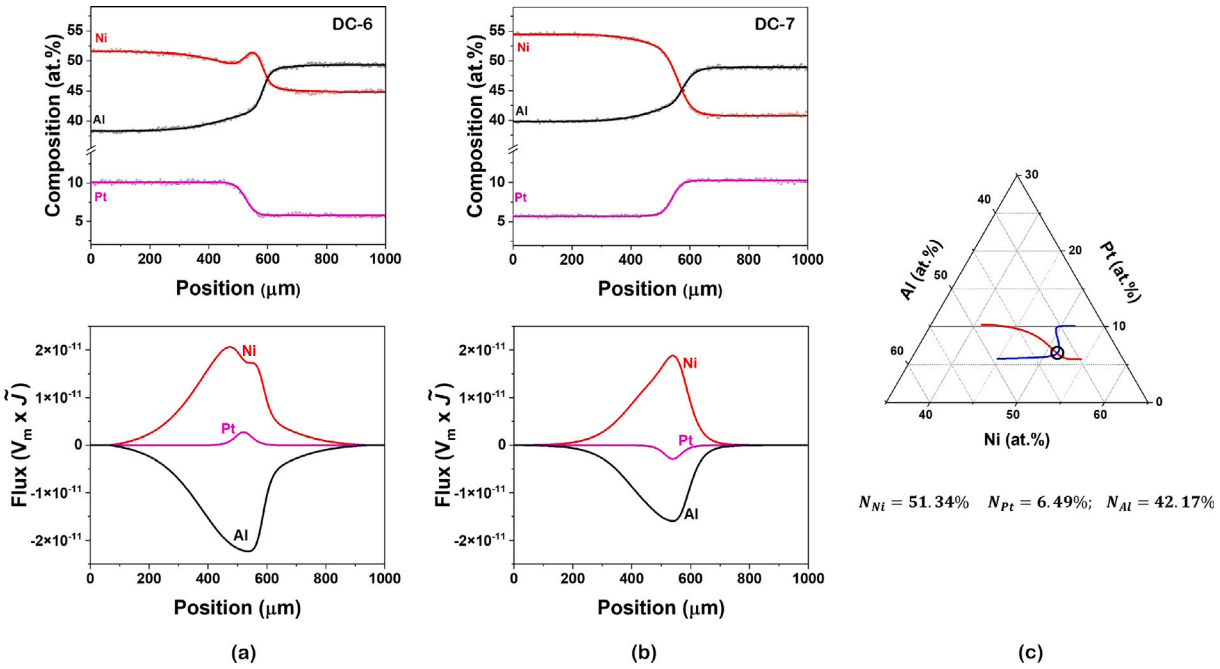

Fig. 11. Composition profiles developed between EMT alloys for (a) DC-6 and (b) DC-7. In (c) the diffusion paths are shown on the Gibbs triangle and the composition corresponding to the intersection of the two composition profiles is indicated.

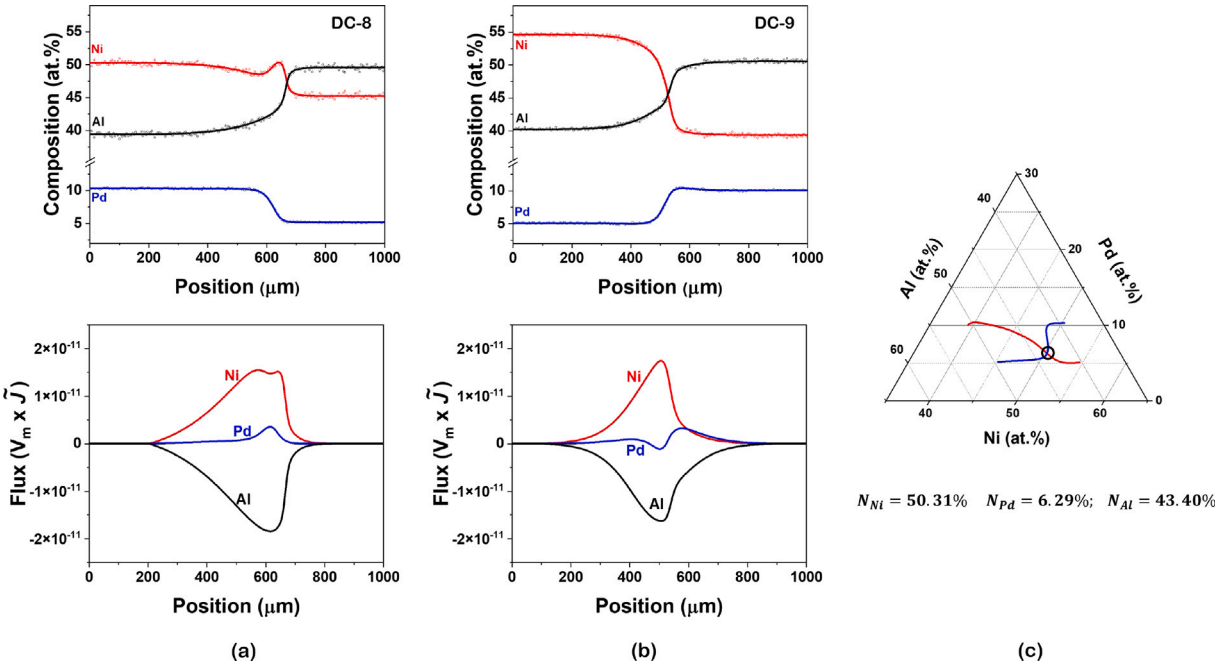

Fig. 12. Composition profiles developed between EMT alloys (a) DC-8 (b) DC-9. In (c) the diffusion paths are shown on the Gibbs triangle and the composition corresponding to the intersection of the two composition profiles is indicated.

temperature, above 0.7 of the melting point, we can safely assume that the grain boundary diffusion contribution is minimal in these experimental results. A very rough estimate can be done following the Hart model [40] of diffusion at high temperatures in the so-called type A kinetics after Harrison classification [41]. Using the grain boundary diffusion data measured for Ni diffusion in NiAl (reported in Ref. [17]), a relative contribution of the grain boundary diffusion transport to the interdiffusion flux can be estimated as less than 0.1 for the grain size of 10 micrometres. Therefore, we need to consider mainly lattice diffusion.

Therefore, the presence of Pt or Pd or both (Pt+Pd) in the bond coat influences the growth rates of the IDZ because of characteristic changes in the interdiffusion coefficients. The diffusion rates of the elements are generally influenced by the following factors:

(*i*) changes of the point defect concentrations assisting the lattice diffusion;
(*ii*) changes of the migration barriers of the vacancy-mediated jumps; and/or
(*iii*) changes of the thermodynamic driving forces.

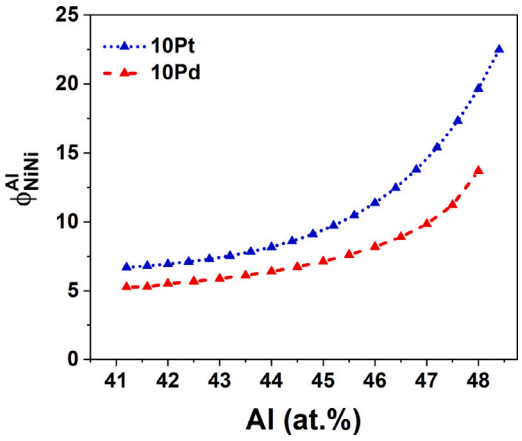

Fig. 13. Thermodynamic factor of Ni at 1373 K in the β-NiAl phase with 10 at.% Pt or 10 at.%Pd addition.

Based on the diffusion analysis in the binary B2-NiAl system [42,43], we already know that the changes in the defect concentrations, mentioned in item (*i*) above, play a dominating role over the thermodynamic driving forces [7], mentioned in item (*iii*). For further clarification, the thermodynamic factor $\phi^{Al}_{NiNi} = \phi_{NiNi} - (N_{Ni}/N_{Al})\phi_{NiAl} = (\partial \ln a_{Ni}/\partial \ln N_{Ni}) - (N_{Ni}/N_{Al})(\partial \ln a_{Ni}/\partial \ln N_{Al})$ along the composition profile of the PB diffusion couples in the presence of Pt or Pd are compared in Fig. 13. Here a_i is the activity of element i, and Al is chosen as the dependent variable. The thermodynamic calculations are carried out in ThermoCalc software 2019a using TCNI9: Ni-based superalloy database, accessed on Jan 2020 [44]. The thermodynamic factor in the presence of Pt is higher than that in the presence of Pd at any composition under investigation. However, the thermodynamic factors increase monotonically with the increasing Al content, although the PB interdiffusion coefficients decrease with the increase of Al content, as shown in Fig. 8. These facts indicate that the changes of the defect concentrations with composition in the presence of Pt or Pd play a major role, potentially alongside the impact of Pt or Pd alloying on the vacancy jump barriers.

3.3. DFT-informed analysis of the diffusion process

Atom diffusion in the B2 phase of NiAl has been extensively measured using radiotracer [45–47] and diffusion couple [48,49] techniques and theoretically assessed in a number of publications, see e.g. [47,50–53]. As a result, the diffusion mechanisms are considered to be well understood [47,51,54]. The so-called triple defects [47,55] and the Ni anti-structure atoms [47] are identified to dominate the tracer diffusion rates of Ni atoms, while Ni vacancies and the triple defects seem to contribute to Al diffusion [51]. A certain contribution of the six-jump cycle mechanism [56], especially at near stoichiometric compositions [57], and of the so-called anti-site bridge mechanism [58] for strongly Ni-rich alloys [47] were identified, too. In this study, we use DFT to calculate the alloying-induced changes of the point defect concentrations in NiAl.

Possible point defects in an ordered B2 lattice of NiAl are illustrated in Fig. 14(a), namely two types of vacancies (V_{Ni} and V_{Al}) and two types of anti-site defects (Ni_{Al} and Al_{Ni}). A triple defect, i.e., $2V_{Ni}+Ni_{Al}$ as a nearest-neighbouring configuration, and the triple defect diffusion mechanism are exemplified in Fig. 14(b). We focus on this defect and mechanism due to its dominant contribution to Ni and Al diffusion in the Ni-rich compositions under investigation [47].

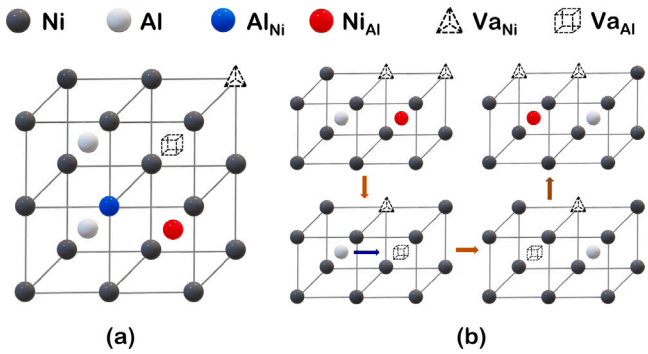

Fig. 14. Point defects in the B2 structure of NiAl (a) and a schematic illustration of the triple defect mechanism with the next nearest neighbour jump (blue arrow) of an Al atom (b).

Table 5
Lattice parameter a, formation energy E_0 (in eV/at), and effective defect formation energies (in eV/point defect) for a binary and ternary system with 10%Pt and 10%Pd. V_{Ni} (V_{Al}) is a vacancy on the specified sublattice.

	B2 NiAl	+10%Pt	+10%Pd
a (Å)	2.893	2.939	2.934
E_0 (eV/at)	−0.662	−0.713	−0.686
Defect (X = Pt/Pd)	Energy (eV/defect)		
V_{Ni}	0.41	0.32	0.38
V_{Al}	1.76	1.12	1.52
V_X	–	0.83	0.65
Ni_{Al}	1.03	0.94	1.00
Al_{Ni}	1.63	1.52	1.55
X_{Ni}	−0.51	0(ref)	0(ref)
X_{Al}	0.55	1.01	0.90
Triple defect	1.84	1.58	1.76

3.3.1. Defect concentrations

The impact of Pd alloying on the defect concentrations in B2 NiAl is evaluated using the two approaches elaborated in Refs. [7] and [54], for which consistent results have been achieved. Pd (and Pt) atoms are known to substitute Ni in B2 NiAl [52,59–61]. The distribution of Pd atoms on the transition metal sub-lattice (Ni, dark spheres in Fig. 14) of the B2 lattice in the ternary NiPdAl phase was generated using the *sqsgen* script integrated in pyiron [62]. Up to two-body correlations were considered to generate the special quasi-random structure (SQS) [63]. A 4 × 4 × 4 repetition of the bcc unit cell was used with 64 Al atoms, 51 Ni atoms, and 13 Pd atoms. These numbers correspond to roughly 40% Ni, 10% Pd, and 50% Al. This supercell was chosen because it is large enough to avoid a significant interaction of the different defects with their periodic images. A sensitivity analysis was performed using additional 3 × 3 × 3 supercell indicating that the defect formation energies are converged to below 0.08 eV.

The DFT calculations were performed at 0 K and finite temperature effects were restricted to the consideration of configurational entropy. The differences in the vibrational entropy effects for the studied systems: B2-NiAl, B2-NiAl+10%Pd, (and B2-NiAl+10%Pt examined previously [7]) are expected to be small, due to the similar chemical nature, the same underlying lattice (B2-type) structure, and the negligible differences in the lattice parameters caused by Pd and Pt alloying, see Table 5.

The calculated formation energies of relevant defects, i.e. vacancies and anti-sites, in the B2 phases of $Ni_{0.5}Al_{0.5}$, $Ni_{0.4}Pd_{0.1}Al_{0.5}$, and $Ni_{0.4}Pt_{0.1}Al_{0.5}$ are listed in Table 5. The defects energies for NiAl+10% Pd are binomial weighted averages of 8 randomly selected chemical configurations next to the respective defect, similar to the previous work [7]. In the same way, we also repeated the calculations of B2 NiAl+10% Pt, but with different SQSs and supercells than in [7], and listed the determined values for the sake of comparison.

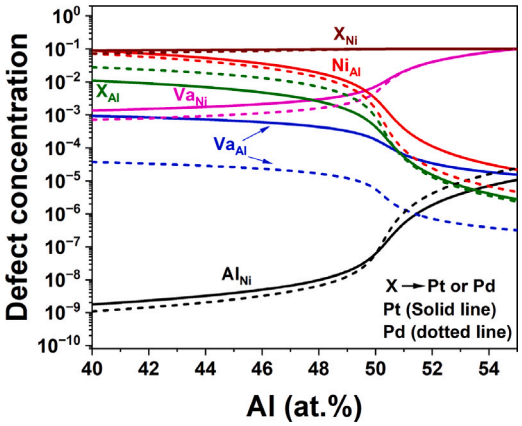

Fig. 15. Comparison of defects concentrations at 1373 K for B2 NiAl+10%Pd (dotted curves) and B2 NiAl+10%Pt (solid curves) as a function of Al concentration.

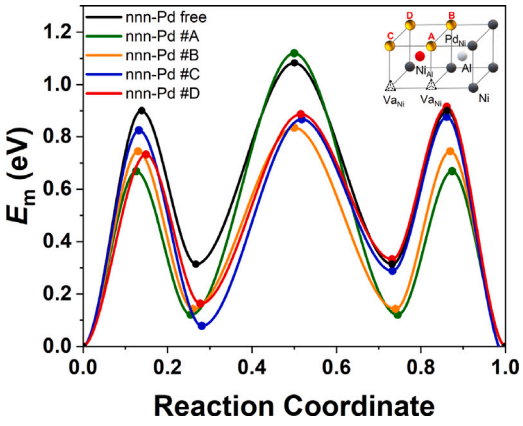

Fig. 16. Minimum energy paths for the triple defect diffusion mechanism by Quasi-Newton calculations for B2 NiAl with Pd substitution at four different sites for nnn jump of Al.

Table 6
Concentrations of triple defects, X_{td}, in binary NiAl and ternary systems with 10%Pt and 10%Pd at 1373 K in alloys with Al = 47.5%.

	B2 NiAl	+10%Pt	+10%Pd
X_{td} (10^{-8})	2.33	17.25	3.71

Table 7
Thickness of the interdiffusion zone (IDZ) in terms of precipitation-containing (prec.) and precipitation-free (free) sublayers developed between a bond coat and CMSX-4 superalloy. For comparison, the results of investigations of Kiruthika et al. [6] on the NiAl/CMSX-4 couple are listed, too. The alloying elements for the NiAl bond coats are indicated.

Diffusion couple	Alloying element	Thickness of IDZ (μm)	
		Prec.	Free
NiAl/CMSX4 [6]	–	16	230
DC-10	Pt	35	245
DC-12	Pt+Pd	26	180
DC-13	Pd	16	96

The defect concentrations are obtained using the computed defect formation energies, rate equations for defect formation and accounting for a mass balance, (see Ref. [7] for details). The results for B2 NiAl are in good agreement with the literature data reported by Korzhavyi and Ruban [64] using a locally self-consistent Green's function method and by Fu et al. [65] using the LDA functional. In Fig. 15, the determined defect concentrations in $Ni_{0.4}Pd_{0.1}Al_{0.5}$ are compared with $Ni_{0.4}Pt_{0.1}Al_{0.5}$ at 1373 K.

For a given (fixed) Al concentration, replacement of Ni by Pt was reported to increase the concentration of Ni vacancies and Ni antisites [7]. The same trends are seen with 10%Pd alloying, but the increments are more moderate. The concentrations of the triple defects are found to be almost composition-independent (for Al-deficit alloys) and the determined values at 1373 K are listed in Table 6. The results support generally the main findings of the present interdiffusion measurements and explain the highest diffusion enhancement in NiAlPt and a moderate one in NiAlPd with respect to binary NiAl.

3.3.2. Migration barriers

The sequence of atomic jumps according to the triple defect jump mechanism in NiAl is shown schematically in Fig. 14(b). The Ni atoms (dark spheres) perform nearest-neighbour jumps between different sublattices and the Al atom (light spheres) performs a next nearest-neighbour jump within its own sublattice. In Fig. S7 in Supplementary the results of computationally expensive nudged elastic band (NEB) calculations [66,67] are compared with a simplified quasi-Newton calculation [68]. The quasi-Newton method is more efficient, as only one image/configuration is needed instead of multiple images, while the NEB method used in our previous work [7] required 5 and 9 images/configurations for the first and second nearest-neighbour jumps, respectively. The NEB method has advantages if the exact migration path (saddle point configuration) is not known, but in the present case of a known migration path, the comparison of the NEB and quasi-Newton calculations, Fig. S2, confirms the applicability of the latter one.

Accordingly, we used the quasi-Newton approach to perform exemplary calculations of the migration energies according to the triple defect mechanism in B2 NiAl with Pd atoms at the positions A, B, C, and D as shown in the image in Fig. 16. The migration barriers, E_m, were determined as the maximum energy barrier between the initial and final configurations. Depending on the position of the Pd atom on the Ni sublattice, the migration energy is generally decreased, Fig. 16, but the decrease is slightly smaller comparing to that seen for the Pt replacement in the same configurations [7]. The reason for this behaviour may be due to the size difference of the elements down the group of the periodic table. The decreased energy barriers promote the diffusion of both Ni and Al, i.e., of all three steps in the jump sequences of the triple defect mechanism, Fig. 14.

3.4. Analysis of the influence of Pt (Pd) on the IDZ grown between the alloyed bond coat and the superalloy

We have first shown that the IDZ thickness decreases with partial or complete replacement of Pt by Pd, which is a major benefit for the reliability or life time of the turbines used in various high-temperature applications. The thickness of precipitate-containing and precipitate-free sublayers of the IDZ are listed in Table 7.

A partial replacement of Pt by Pd has a beneficial role in view of (i) an expected spallation resistance similar to the bond coat containing Pt only [12] and (ii) inhibiting the growth of deleterious $(Pt,Ni)Al_2$ precipitates during the pack cementation process [16]. In the present study, the significant (and beneficial) change of the diffusion-controlled growth of the IDZ is quantitatively analysed by following the pseudo-binary diffusion couple method in the Pt- and Pd-containing ternary and quaternary B2-NiAlPtPd alloys. The PB-interdiffusion coefficient is found to decrease in the presence of Pd. Furthermore, the ternary diffusion couple experiments in the NiAlPt and NiAlPd alloys indicate a decrease in the interdiffusion rates in the presence of Pd compared to Pt. The impact of Pt or Pd alloying on the diffusion coefficients cannot be explained by considering solely thermodynamic driving forces since the thermodynamic factors and the diffusion coefficients reveal opposite trends of their functional dependencies on the variation

of Al concentration in the alloy. This indicates a dominant role in corresponding changes in defect formation and migration energies.

A full analysis of the diffusion phenomena and their characteristic parameters in a quantitative way in the alloyed NiAl system requires a massive spectrum of work, not just by experiment but also by computations. In the present study, a combination of the DFT-informed calculations of the defect formation and migration energies and the evaluation of the thermodynamic factors based on a thermodynamic assessment provides valuable insights into the impact of alloying on IDZ growth. The interdiffusion coefficients are related to the intrinsic diffusion coefficients by [69],

$$\tilde{D}_{\mathrm{PB}} = M_{\mathrm{Al}} D^{\mathrm{Al}}_{\mathrm{NiNi}} + M_{\mathrm{Ni}} D^{\mathrm{Ni}}_{\mathrm{AlAl}}, \tag{5}$$

where $D^{\mathrm{Al}}_{\mathrm{NiNi}}$ and $D^{\mathrm{Ni}}_{\mathrm{AlAl}}$ are the main intrinsic diffusion coefficients of Ni and Al respectively, and M_{Al} and M_{Ni} are the modified composition parameters introduced in Section 3.2.

In order to simplify the analysis, we will concentrate on the *relative* changes of the interdiffusion coefficients due to alloying, considering the ratios $\tilde{D}^{\mathrm{X}}_{\mathrm{PB}}/\tilde{D}_{\mathrm{NiAl}}$ with X = Pd or Pt and $\tilde{D}_{\mathrm{NiAl}}$ being the interdiffusion coefficient in the binary NiAl alloy. The alloying elements are assumed to occupy the Ni sublattice, and the interdiffusion coefficients are compared at the same Al concentration in the alloy. The intrinsic diffusion coefficients, D^{j}_{ii}, are related to the corresponding tracer diffusion coefficients, D^{*}_{i}, by $D^{j}_{ii} = D^{*}_{i}\phi_i W_i$, where ϕ_i is the thermodynamic factor and W_i is the vacancy wind factor for the element i.

As an additional approximation, we will take into account that in the binary NiAl alloy Ni diffusion dominates over Al to contribute the interdiffusion coefficients [42,43,47,70,71]. Thus, the thermodynamic factor of Ni, $\phi^{\mathrm{Al}}_{\mathrm{NiNi}} = \phi_{\mathrm{Ni}}$, Fig. 13, has to be considered. Further, the contributions of the vacancy wind factors (which are about unity [70, 72]) are neglected. Then the impact of alloying on the interdiffusion coefficient is reduced to

$$\frac{\tilde{D}^{\mathrm{X}}_{\mathrm{PB}}}{\tilde{D}_{\mathrm{NiAl}}} \approx \frac{D^{*}_{\mathrm{Ni}}(\mathrm{NiAlX})}{D^{*}_{\mathrm{Ni}}(\mathrm{NiAl})} \frac{\phi_{\mathrm{Ni}}(\mathrm{NiAlX})}{\phi_{\mathrm{Ni}}(\mathrm{NiAl})}. \tag{6}$$

Generally, tracer diffusion in an ordered intermetallic compound is determined not only by vacancies but also by further point defects δ, with $\delta = V_{\mathrm{Ni}}$, V_{Al}, $\mathrm{Ni_{Al}}$, $\mathrm{Al_{Ni}}$, $\mathrm{X_{Ni}}$, $\mathrm{X_{Al}}$ in the particular case of B2 NiAl-X, since the given state of ordering is maintained during thermal diffusion. The tracer diffusion coefficient of Ni in B2 NiAl, which in fact corresponds to a multi-barrier process of vacancy-mediated atomic jumps, can be presented as induced by a one-barrier process with an effective energy of migration, E^{eff}_{m}, [17]

$$D^{*}_{\mathrm{Ni}} = g a^2 f_{\mathrm{Ni}}(T) \nu_0 \exp\left(-\frac{\Delta H^{f}_{V_{\mathrm{Ni}}} + \Delta H^{f}_{\delta} + \Delta H^{b}}{k_B T}\right) \times \exp\left(-\frac{E^{eff}_{m}}{k_B T}\right). \tag{7}$$

Here, g is a geometrical factor, which is unity in a cubic lattice, a is the lattice parameter, $f_{\mathrm{Ni}}(T)$ is the temperature-dependent correlation factor, ν_0 is the attempt frequency, ΔH^{f}_{δ} is the (total) formation enthalpy of the involved defect(s) indexed by δ in addition to the Ni vacancy V_{Ni}, ΔH^{b} is the corresponding binding energy between the defect(s) and the Ni vacancy, V_{Ni}. Note that the tracer correlation factor, particularly f_{Ni}, is temperature-dependent and can provide a large contribution to the effective activation energy of diffusion, up to 30% in some cases [17], thus accounting for correlations during atom jumps following a multi-barrier process.

In the case of B2 ordered NiAl, the triple defect diffusion mechanism, Fig. 14(b), has been identified as a dominating one, especially at the compositions close to stoichiometry [47]. Then, in view of Eq. (7) and explicitly neglecting the correlation effects, Eq. (6) is further simplified to

$$\frac{\tilde{D}^{\mathrm{X}}_{\mathrm{PB}}}{\tilde{D}_{\mathrm{NiAl}}} \approx \frac{X_{\mathrm{td}}(\mathrm{NiAlX})}{X_{\mathrm{td}}(\mathrm{NiAl})} \times \frac{\phi_{\mathrm{Ni}}(\mathrm{NiAlX})}{\phi_{\mathrm{Ni}}(\mathrm{NiAl})} \times \exp\left(-\frac{\left[E^{eff}_{m}(\mathrm{NiAlX}) - E^{eff}_{m}(\mathrm{NiAl})\right]}{k_B T}\right). \tag{8}$$

Thus, the impact of alloying on interdiffusion is decomposed into a product of three basic contributions, i.e., the defect concentrations (in the present case, the triple defect concentration X_{td} has to be accounted for), the thermodynamic factors and the changes of the effective migration barriers. An exact quantitative assessment may be a subject of a separate study. However, the present semi-quantitative analysis provides fundamental understanding of the interdiffusion rates required for a further development of the bond coat superalloy systems.

The estimates below are exemplified for the composition of 47.5 at.% of Al and T = 1373 K. Using the DFT input, the Pt alloying is estimated to increase the interdiffusion coefficient by a factor of $7.40 \times 0.98 \times 9.23 \approx 66.9$ with respect to that in binary NiAl, while $\tilde{D}^{\mathrm{Pd}}_{\mathrm{PB}}/\tilde{D}_{\mathrm{NiAl}} = 1.59 \times 0.67 \times 6.26 \approx 6.67$. Astonishingly, despite of all approximations, the relative enhancement of the interdiffusion rate due to the Pt alloying with respect to that by the Pd addition is in good agreement with experiment, Fig. 8.

Experimentally, Pt addition is found to increase the interdiffusion coefficients by a factor of 6, while Pd retards interdiffusion to about 60% of the value for binary B2 NiAl. Thus, experimentally, the Pd alloying decreases the diffusion rates by a factor of 10 comparing to the impact of equivalent Pt addition, $\tilde{D}^{\mathrm{Pt}}_{\mathrm{PB}}/\tilde{D}^{\mathrm{Pd}}_{\mathrm{PB}} \approx 10$. Eq. (8) predicts a similar factor accounting for the contributions from the defect formation and migration and the thermodynamic factors, since $\left(\tilde{D}^{\mathrm{Pt}}_{\mathrm{PB}}/\tilde{D}^{\mathrm{Pd}}_{\mathrm{PB}}\right)_{\mathrm{DFT}}$ is estimated at about 10, too. Thus, the DFT-informed analysis indeed supports the explanation of the alloying effect in terms of the defect concentrations.

An analysis of individual contributions to Eq. (8) indicates that at least for the atomic configurations studied, Pt or Pd alloying influence the diffusion barriers of neighbouring Ni atoms similarly, while their impacts on the defect concentrations in NiAl, Table 6, are different.

The present analysis, Eq. (8), overestimates the impact of alloying by a factor of ten. Most probably, Pt or Pd alloying enhances kinetic correlations of vacancy-mediated atomic jumps reducing the value of the corresponding correlation factor $f_{\mathrm{Ni}}(\mathrm{NiAlX})$ with respect to that in binary NiAl (this contribution is neglected in Eq. (8)). Such an explanation agrees with the predicted decrease of the energy barriers of Ni atom jumps in the neighbourhood of alloying atoms, Fig. 16. This results in an additional (kinetic) binding of vacancies towards the alloying atoms and retardation of long-range diffusion of the matrix atoms. Therefore, a full analysis extending the approach elaborated, e.g., by Van der Ven et al. [53,73] for binary NiAl and including a proper kinetic Monte-Carlo calculations is required.

Therefore, the combined experimental-theoretical study correlates successfully the characteristic changes in the thickness of IDZ grown between the bond coat and the superalloy with the results of the quantitative diffusion analysis and the DFT-informed calculations.

4. Conclusions

Pd and Pt alloying effects on the interdiffusion coefficients are investigated by the PB method and the conventional Matano-Kirkaldy approach in the β-NiAl intermetallic compound. The estimated interdiffusion coefficients are compared, and the diffusional interactions between the constituting elements are discussed.

1. A partial or complete replacement of Pt with Pd is found to reduce the PB interdiffusion coefficient of Ni and Al. This also reflects on the reduced growth rate of the interdiffusion zone between the bond coat and the superalloy because of Pd addition.

2. The combined alloying by Pd+Pt follows a similar trend as that for solely Pd addition to B2-NiAl on the variation of interdiffusion coefficients with composition. The diffusion coefficients are almost similar for both up to 46 at.% Al. At higher Al content towards the stoichiometry, the PB interdiffusion coefficients are higher in Pd+Pt alloys than in the Pd-containing alloys.
3. The estimation of the ternary interdiffusion coefficients indicates that the main interdiffusion coefficients of Ni, i.e. $\tilde{D}^{Al}_{NiNi}$ (see Table 4) and Al, i.e. $\tilde{D}^{Ni}_{AlAl}$ (see supplementary file) are higher in presence of Pt compared to Pd.
4. DFT calculations revealed that for the atomic configurations studied, Pt or Pd alloying influence the diffusion barriers of neighbouring Ni atoms similarly, while their impacts on the defect concentrations in NiAl are different.
5. Pd exhibits uphill diffusion in the interdiffusion zone when it diffuses in the same direction as Al and is opposite to Ni (see Fig. 11b). However, Pt does not show a similar effect (see Fig. 10b). Other characteristics of the diffusion profiles are similar (see Figs. 10c and 11c), although the interdiffusion zone lengths are different.
6. The quantitative EPMA elemental mapping and the TEM analyses elucidated the nature of the TCP phases formed in the interdiffusion zones. The growth of σ-, R- and μ-phases is not impeded by alloying with both, Pt or Pd.

It should be noted here that this article did not aim to find the optimized composition of Pt and Pd for overall improved properties, which is a multi-factorial optimization process and would include not only the diffusion but a number of further aspects. The objective of this article was to understand the underlying diffusion-controlled growth of the interdiffusion zone that leads to unwanted loss of Al. The analysis and understanding developed in this article covers Pt, Pd and Pt-Pd (with equal proportions) containing bond coats, but this be extended to any other relative Pt/Pd concentrations.

Declaration of competing interest

The authors declare that they have no known competing financial interests or personal relationships that could have appeared to influence the work reported in this paper.

Acknowledgements

AP and VJ acknowledge the financial support from ARDB, India, grant number: ARDB/GTMAP/01/2031786/M. SD and TH acknowledge a partial financial support from the German Research Foundation (DFG).

Appendix A. Supplementary data

Supplementary material related to this article can be found online at https://doi.org/10.1016/j.actamat.2024.119687.

References

[1] J.A. Haynes, B.A. Pint, K.L. More, Y. Zhang, I.G. Wright, Influence of sulfur, platinum, and hafnium on the oxidation behavior of CVD NiAl bond coatings, Oxid. Met. 58 (2002) 513–544.
[2] D.K. Das, Microstructure and high temperature oxidation behavior of Pt-modified aluminide bond coats on Ni-base superalloys, Prog. Mater. Sci. 58 (2) (2013) 151–182.
[3] B. Nagamani Jaya, Micro-scale fracture testing of graded (Pt, Ni) Al bond coats (Ph.D. thesis), Ph.D. thesis, Indian Institute of Science, Bangalore, 2013.
[4] S. Hayashi, S.I. Ford, D.J. Young, D.J. Sordelet, M.F. Besser, B. Gleeson, α-NiPt(Al) and phase equilibria in the Ni–Al–Pt system at 1150 °C, Acta Mater. 53 (2005) 3319–3328.
[5] G.R. Krishna, D.K. Das, V. Singh, S.V. Joshi, Role of pt content in the microstructural development and oxidation performance of Pt–aluminide coatings produced using a high-activity aluminizing process, Mater. Sci. Eng. A 251 (1-2) (1998) 40–47.
[6] P. Kiruthika, S.K. Makineni, C. Srivastava, K. Chattopadhyay, A. Paul, Growth mechanism of the interdiffusion zone between platinum modified bond coats and single crystal superalloys, Acta Mater. 105 (2016) 438–448.
[7] N. Esakkiraja, A. Gupta, V. Jayaram, T. Hickel, S.V. Divinski, A. Paul, Diffusion, defects and understanding the growth of a multicomponent interdiffusion zone between Pt-modified B2 NiAl bond coat and single crystal superalloy, Acta Mater. 195 (2020) 35–49.
[8] D.K Das, V. Singh, S.V Joshi, Effect of Al content on microstructure and cyclic oxidation performance of Pt-aluminide coatings, Oxid. Met. 57 (2002) 245–266.
[9] B. Grushko, Again regarding the Al–Pd phase diagram, J. Alloys Compd. 557 (2013) 102–111.
[10] H. Okamoto, Supplemental literature review of binary phase diagrams: Al-Pt, As-U, C-Li, C-Mg, Cd-Nd, Co-Ta, Fe-Re, Ga-Y, La-Ni, O-V, P-Si, and Re-Zr, J. Phase Equilibria a Diff. 41 (2020) 722–733.
[11] P. Lamesle, P. Steinmetz, J. Steinmetz, S. Alpérine, Palladium-modified aluminide coatings: Mechanisms of formation, J. Electrochem. Soc. 142 (1995) 497–505.
[12] T. Baskaran, N. Esakkiraja, C. Samartha, P. Kumar, V. Jayaram, A. Paul, Effect of addition of Pt, Pd and Ir to β-NiAl-bond coat on oxidation resistance and growth of interdiffusion zone, Surf. Coat. Technol. 426 (2021) 127766.
[13] Raghavendra R. Adharapurapu, Jun. Zhu, Voramon S. Dheeradhada, Don M. Lipkin, Tresa M. Pollock, A combinatorial investigation of palladium and platinum additions to β-NiAl overlay coatings, Acta Mater. 77 (2014) 379–393.
[14] M. Góral, M. Pytel, T. Kubaszek, M. Drajewicz, W. Simka, Ł. Nieużyła, The new concept of thermal barrier coatings with Pt + Pd/Zr/Hf-modified aluminide bond coat and ceramic layer formed by PS-PVD method, High Temp. Mater. Process. 40 (2021) 281–286.
[15] J. Romanowska, J. Morgiel, M. Zagula-Yavorska, The influence of Pd and Zr co-doping on the microstructure and oxidation resistance of aluminide coatings on the CMSX-4 nickel superalloy, Materials 14 (2021) 7579.
[16] S.J. Hong, G.H. Hwang, W.K. Han, S.G. Kang, Cyclic oxidation of Pt/Pd-modified aluminide coating on a nickel-based superalloy at 1150°C, Intermetallics 17 (6) (2009) 381–386.
[17] S. Divinski, Chapter 10 - defects and diffusion in ordered compounds, in: Handbook of Solid State Diffusion, Vol. 1, Elsevier, 2017, pp. 449–517.
[18] D. Gärtner, L. Belkacemi, V.A. Esin, F. Jomard, A.A. Fedotov, J. Schell, J.V. Osinskaya, A.V. Pokoev, C. Duhamel, A Paul, S.V. Divinski, Techniques of tracer diffusion measurements in metals, alloys and compounds, Diff. Found. 29 (2021) 31–73.
[19] N. Esakkiraja, K. Pandey, A. Dash, A. Paul, Pseudo-binary and pseudo-ternary diffusion couple methods for estimation of the diffusion coefficients in multicomponent systems and high entropy alloys, Phil. Mag. 99,18 (2019) 2236–2264.
[20] A. Paul, A pseudobinary approach to study interdiffusion and the Kirkendall effect in multicomponent systems, Phil. Mag. 93,18 (2013) 2297–2315.
[21] G. Kresse, J. Hafner, Ab initio molecular dynamics for liquid metals, Phys. Rev. B 47 (1993) 558–561.
[22] G. Kresse, J. Furthmüller, Efficient iterative schemes for ab initio total-energy calculations using a plane-wave basis set, Phys. Rev. B 54 (1996) 11169–11186.
[23] J.P. Perdew, K. Burke, M. Ernzerhof, Generalized gradient approximation made simple, Phys. Rev. Lett. 77 (1996) 3865–3868.
[24] H.J. Monkhorst, J.D. Pack, Special points for Brillouin-zone integrations, Phys. Rev. B 13 (1976) 5188–5192.
[25] M. Methfessel, A.T. Paxton, High-precision sampling for Brillouin-zone integration in metals, Phys. Rev. B 40 (1989) 3616–3621.
[26] M.J Li, X.F Sun, H.R Guan, X.X Jiang, Z.Q Hu, Cyclic oxidation behavior of palladium-modified aluminide coating, Surf. Coat. Technol. 167,1 (2003) 106–111.
[27] A. Paul, T. Laurila, V. Vuorinen, S.V. Divinski, Thermodynamics, Diffusion and the Kirkendall Effect in Solids, Springer Int. Publ. Switzerland, 2014.
[28] C. Ghosh, A. Paul, A physico-chemical approach in binary solid-state interdiffusion, Acta Mater. 55,6 (2007) 1927–1939.
[29] C.M.F. Rae, R.C. Reed, The precipitation of topologically close-packed phases in rhenium-containing superalloys, Acta Mater. 49,19 (2001) 4113–4125.
[30] A. Paul, Chapter 3 - estimation of diffusion coefficients in binary and pseudo-binary bulk diffusion couples, handbook of solid state diffusion, volume 1, in: Handbook of Solid State Diffusion. Vol. 1, Elsevier, 2017, pp. 79–201.
[31] Guido Schmitz, Constantin-Buzau Ene, Carsten Nowak, Reactive diffusion in nanostructures of spherical symmetry, Acta Mater. 57 (9) (2009) 2673–2683.
[32] G.Brian Stephenson, Deformation during interdiffusion, Acta Metall. 36 (10) (1988) 2663–2683.
[33] Z. Erdélyi, B. Parditka, D.L. Beke, Stress effects on the kinetics of nanoscale diffusion processes, Scr. Mater. 64 (10) (2011) 938–941.
[34] J.S. Kirkaldy, Diffusion in multicomponent metallic systems: I. Phenomenological theory for substitutional solid solution alloys, Can. J. Phys. 36 (7) (1958) 899–906.
[35] A. Paul, Comments on sluggish diffusion in Co–Cr–Fe–Mn–Ni high-entropy alloys, Scr. Mater. 135 (2017) 153–157.

[36] H. Kumar, A. Dash, A. Paul, S. Bhattacharyya, A physics-informed neural network-based numerical inverse method for optimization of diffusion coefficients in NiCoFeCr multi principal element alloy, Scr. Mater. 214 (2022) 114639.
[37] M. Seyring, M. Rettenmayr, Impact of crystallography at Ni/NiAl interfaces on the nucleation of Ni3Al, Acta Mater. 208 (2021) 116713.
[38] J.S Kirkaldy, D. young, Diffusion in the Condensed State, The Institute of Metals, London, United Kingdom, 1987.
[39] U. Bansal, A. Srivastava, N. Esakkiraja, Tamilselvi M, A. Paul, Effect of pt on diffusion-controlled growth characteristics of interdiffusion zone between CM247LC superalloy and Ni(Pt)Al bond coat, J. Mater. Sci. 58 (3) (2023) 1305–1314.
[40] E.W. Hart, On the role of dislocations in bulk diffusion, Acta Metall. 5 (10) (1957) 597.
[41] L.G. Harrison, Influence of dislocations on diffusion kinetics in solids with particular reference to the alkali halides, Trans. Faraday Soc. 57 (1961) 1191–1199.
[42] A. Paul, A.A. Kodentsov, F.J.J. van Loo, Bifurcation of the Kirkendall plane during interdiffusion in the intermetallic compound beta-NiAl, Acta Mater. 52 (2004) 4041–4048.
[43] A. Paul, A.A. Kodentsov, F.J.J. van Loo, On diffusion in the β-NiAl phase, J. Alloys Compd. 52 (2005) 147–153.
[44] J-O Andersson, T. Helander, L. Höglund, P. Shi, B. Sundman, Thermo-calc & DICTRA, computational tools for materials science, CALPHAD 26 (2) (2002) 273–312.
[45] G.F. Hancock, B.R. McDonnel, Diffusion in the intermetallic compound NiAl, Phys. Status Solidi (a) 4 (1971) 143–150.
[46] A. Lutze-Birk, H. Jacobi, Diffusion of ^{114m}in in NiAl, Scr. Metall. 9 (1975) 761–765.
[47] St Frank, S.V Divinski, U. Södervall, Chr Herzig, Ni tracer diffusion in the B2-compound NiAl: Influence of temperature and composition, Acta Mater. 49 (2001) 1399–1411.
[48] Y. Minamino, Y. Koizumi, N. Tsuji, M. Morioka, K. Hirao, Y. Shirai, Pt diffusion in B2-type ordered NiAl intermetallic compound and its diffusion mechanisms, Sci. Technol. Adv. Mater. 1 (2000) 237–249.
[49] Y. Minamino, Y. Koizumi, Y. Inui, In diffusion in B2-type ordered NiAl intermetallic compound, in: Diffusion in Materials DIMAT2000, in: Defect and Diffusion Forum, vol.194, Trans Tech Publications Ltd, 2001, pp. 517–522.
[50] Y. Mishin, D. Farkas, Atomistic simulation of point defects and diffusion in B2 NiAl, Phil. Mag. A 75 (1997) 187–199.
[51] Y. Mishin, A.Y. Lozovoi, A. Alavi, Evaluation of diffusion mechanisms in NiAl by embedded-atom and first-principles calculations, Phys. Rev. B 67 (2003) 014201.
[52] K.A. Marino, E.A. Carter, The effect of platinum on defect formation energies in β-NiAl, Acta Mater. 56, 14 (2008) 3502–3510.
[53] Q. Xu, A. Van der Ven, Atomic transport in ordered compounds mediated by local disorder: Diffusion in $B2$-Ni_xAl_{1-x}, Phys. Rev. B 81 (2010) 064303.
[54] H.I. Sözen, E. Mendive-Tapia, T. Hickel, J. Neugebauer, Ab initio investigations of point and complex defect structures in B2-FeAl, Phys. Rev. Mater. 6 (2022).
[55] H. Bakker, N.A. Stolwijk, M.A. Hoetjes-eijkel, Diffusion kinetics and isotope effects for atomic migration via divacancies and triple defects in the CsCl (B2) structure, Philosop. Mag. A: Phys. Condensed Matter Struct. Defects Mech. Propert. 43 (1981) 251–264.
[56] E.W. Elcock, C.W. McCombie, Vacancy diffusion in binary ordered alloys, Phys. Rev. 109 (1958) 605.
[57] S. Divinski, Chr. Herzig, On the six-jump cycle mechanism of self-diffusion in NiAl, Intermetallics 8 (12) (2000) 1357–1368.
[58] C.R. Kao, Y.A. Chang, On the composition dependencies of self-diffusion coefficients in B2 intermetallic compounds, Intermetallics 1 (4) (1993) 237–250.
[59] Balasubramanian M., Pease D.M., Budnick J.I., Manzur T., Brewe D.L., Site-occupation tendencies for ternary additions (Fe, Co, Ni) in β-phase transition-metal aluminides, Phys. Rev. B 51, 13 (1995) 8102–8106.
[60] C. Jiang, M. Besser, D.J. Sordelet, B.M. Gleeson, A combined first-principles and experimental study of the lattice site preference of Pt in B2 NiAl, Acta Mater. 53 (2005) 2101–2109.
[61] C. Jiang, Site preference of transition-metal elements in B2 NiAl: A comprehensive study, Acta Mater. 55, 14 (2007) 4799–4806.
[62] J. Janssen, S. Surendralal, Y. Lysogorskiy, M. Todorova, T. Hickel, R. Drautz, J. Neugebauer, Pyiron: An integrated development environment for computational materials science, Comput. Mater. Sci. 163 (2019) 24–36.
[63] A. Zunger, S.-H. Wei, L.G. Ferreira, J.E. Bernard, Special quasirandom structures, Phys. Rev. Lett. 65,3 (1990) 353–356.
[64] P.A. Korzhavyi, A.V. Ruban, A.Y. Lozovoi, Yu. Kh. Vekilov, I.A. Abrikosov, B. Johansson, Constitutional and thermal point defects in $B2$ NiAl, Phys. Rev. B 61 (2000) 6003–6018.
[65] C.L. Fu, Y.-Y. Ye, M.H. Yoo, K.M. Ho, Equilibrium point defects in intermetallics with the B2 structure: NiAl and FeAl, Phys. Rev. B 48 (1993) 6712–6715.
[66] G. Henkelman, B.P. Uberuaga, H. Jónsson, A climbing image nudged elastic band method for finding saddle points and minimum energy paths, J. Chem. Phys. 113,22 (2000) 9901–9904.
[67] G. Henkelman, H. Jónsson, Improved tangent estimate in the nudged elastic band method for finding minimum energy paths and saddle points, J. Chem. Phys. 113,22 (2000) 9978–9985.
[68] C. Freysoldt, On-the-fly parameterization of internal coordinate force constants for quasi-Newton geometry optimization in atomistic calculations, Comput. Mater. Sci. 133 (2017) 71–81.
[69] N. Esakkiraja, A. Dash, A. Mondal, K.C. Hari Kumar, A. Paul, Correlation between estimated diffusion coefficients from different types of diffusion couples in multicomponent system, Materialia 16 (2021) 101046.
[70] Sergiy V. Divinski, Christian Herzig, Ni tracer self-diffusion, interdiffusion and diffusion mechanisms in nial, in: Defects and Diffusion in Metals IV, in: Defect and Diffusion Forum, vol.203, Trans Tech Publications Ltd, 2002, pp. 177–192.
[71] T.R. Paul, Irina V. Belova, E.V. Levchenko, A.V. Evteev, G.E. Murch, Determining a tracer diffusivity by way of the Darken-Manning equation for interdiffusion in binary alloy systems, Diff. Found. 4 (2015) 25–54.
[72] Irina V. Belova, Graeme E. Murch, The vacancy-wind factor and the manning factor occurring in interdiffusion and ionic conductivity in solids, Diff. Found. 22 (2019) 170–183.
[73] A. Van der Ven, H. Yu, G. Ceder, K. Thornton, Vacancy mediated substitutional diffusion in binary crystalline solids, Prog. Mater. Sci. 55 (2010) 61–105.